

On-board Communication-based Relative Localization for Collision Avoidance in Micro Air Vehicle teams

Mario Coppola^{1,2} · Kimberly N. McGuire¹ ·
Kirk Y.W. Scheper¹ · Guido C.H.E. de Croon¹

Received: 14 February 2017 / Accepted: date

Abstract Micro Air Vehicles (MAVs) will unlock their true potential once they can operate in groups. To this end, it is essential for them to estimate on-board the relative location of their neighbors. The challenge lies in limiting the mass and processing burden needed to enable this. We developed a relative localization method that only requires the MAVs to communicate via their wireless transceiver. Communication allows the exchange of on-board states (velocity, height, and orientation), while the signal-strength provides range data. These quantities are fused to provide a full relative location estimate. We used our method to tackle the problem of collision avoidance in tight areas. The system was tested with a team of AR.Drones flying in a 4m×4m area and with miniature drones of $\approx 50g$ in a 2m×2m area. The MAVs were able to track their relative positions and fly several minutes without collisions. Our implementation used Bluetooth to communicate between the drones. This featured significant noise and disturbances in signal-strength, which worsened as more drones were added. Simulation analysis suggests that results can improve with a more suitable transceiver module.

M. Coppola
E-mail: m.coppola@tudelft.nl

K.N. McGuire
E-mail: k.n.mcguire@tudelft.nl

K.Y.W. Scheper
E-mail: k.y.w.scheper@tudelft.nl

G.C.H.E de Croon
E-mail: g.c.h.e.decroon@tudelft.nl

¹Delft University of Technology, Faculty of Aerospace Engineering Department of Control and Simulation (Micro Air Vehicle Laboratory). Kluyverweg 1, 2629HS, Delft, The Netherlands.

²Delft University of Technology, Faculty of Aerospace Engineering Department of Space Systems Engineering. Kluyverweg 1, 2629HS, Delft, The Netherlands.

Keywords Relative Localization · Collision Avoidance · Micro Air Vehicles · Autonomous Flight · Indoor Exploration · Swarm

1 Introduction

The agility and small scale of Micro Air Vehicles (MAVs) make them ideal for indoor exploration (Kumar and Michael, 2012). We imagine several autonomous MAVs navigating through a building/house for mapping or inspection. The swarm could spread out and thus complete the task in a short time. This approach would also bring robustness, scalability, and flexibility to the system, being no longer tied to the success and ability of only one unit (Brambilla et al, 2013). During this scenario, however, it may happen that a few MAVs end up flying together in a small area (e.g. a common bedroom, office, meeting room, hallway), leading to a significant risk of intra-swarm collisions (Szabo, 2015). This is a failure condition to be avoided to ensure mission success without the unwanted loss of units. We have developed and tested a method to tackle this issue which uses only wireless communication between MAVs. Two or more MAVs estimate their relative location via the wireless connection and adjust their path to avoid collisions. In this paper, we describe the details of the algorithm and present real-world results on autonomous drones.

The primary contribution in this article is an on-board relative localization method for MAVs based on intra-swarm wireless communication. The communication channel is used as a method for the exchange of own state measurements and as a measure of relative range (based on signal strength), this provide each MAV sufficient data to estimate the relative location of another. Our implementation uses Bluetooth, which is readily available at a low mass, power, and cost

penalty even on smaller MAVs (McGuire et al, 2016). The advantages of our solution are: a) it provides direct MAV-to-MAV relative location estimates at all relative bearings; b) it has a low dependence on the lighting and sound conditions of the environment; c) it has low mass, battery, and processing requirements; d) it does not require the use of dedicated sensors. The findings also apply to other indoor localization problems, because it shows that only one access point is sufficient to obtain a localization estimate, as opposed to multiple ones in current state of the art (Malyavej et al, 2013; Choudhry et al, 2017). *The secondary contribution is a reactive collision avoidance strategy that is easily tailored to the anticipated performance of the localization estimates.* The strategy was inspired by the concept of collision cones (Fiorini and Shiller, 1998), tailored to suit the expected relative localization performance.

The paper is organized as follows. First, we review a set of related literature in Sect. 2, exploring other approaches towards our goal. Then Sect. 3 introduces the communication-based relative localization methodology, and Sect. 4 describes our collision avoidance strategy. To test the system, we developed a representative room exploration task, explained in Sect. 5. We gradually detail the experiments and results that have been performed, starting from simulation (Sect. 6) to real-world fully autonomous drones (Sect. 8), with positive results. All results are further discussed in Sect. 10. Concluding statements and future challenges are laid out in Sect. 11.

2 Related Work and Research Context

MAVs should be designed to be as efficient as possible to decrease mass and maximize flight-time. This means that they are often limited in sensing, computational power, and payload capabilities (Remes et al, 2014; Mulgaonkar et al, 2015). Collision avoidance is important for mission success but it must not exhaust the already limited resources, which should remain free to pursue the real mission. Arguably, the simplest method to avoid collisions is to have the MAVs fly at different heights. However, experiments by Powers et al (2013) have shown that MAV multi-rotors flying on top of each-other are subject to considerable aerodynamic disturbances. Furthermore, height sensor (e.g. sonar) readings could be disturbed. Based on this limitation, we conclude that lateral evasive maneuvers are needed, and these require relative location estimates between MAVs.

One method to achieve relative localization is to provide a shared reference frame in which each MAV knows its own absolute location. The MAVs can share absolute pose data and infer a relative estimate. In outdoor tasks, Global Positioning System (GPS) receivers can be used to

obtain global position data to share. This has enabled formation flying (Min and Nam, 2016) and large-scale flocking (Vásárhelyi et al, 2014). In indoor tasks, where GPS is not available, absolute position data can be measured using external sensors/beacons in a known configuration, such as: motion tracking cameras (Michael et al, 2010), fixed wireless transmitters/receivers (Guo et al, 2016b; Ledergerber et al, 2015), or visual markers (Faigl et al, 2013). However, these solutions are unsuitable for indoor exploration tasks because they rely on a pre-arranged environment. Simultaneous Localization and Mapping (SLAM) methods circumvent this by generating an indoor map on-board during flight, which then provide position information that can be shared (Scaramuzza et al, 2014). However, if on-board map generation is not part of the mission, then this is a resource intensive practice to be discouraged (Ho et al, 2015). Therefore, the more direct strategy is for the MAVs to directly localize each-other.

To this end, vision has received significant attention, where front-facing cameras are used to detect and localize other MAVs. Current implementations generally adopt mounted visual aids in the form of: colored balls (Roelofsen et al, 2015), tags (Conroy et al, 2014), or markers (Nageli et al, 2014). However, experiments during exploratory phases of this study have shown that using vision without such aids, for very small drones, and at low resolution (128×96px, as seen on the Lisa-S Ladybird (McGuire et al, 2016)) is prone to false-positives/false-negatives. Other disadvantages of using vision are: dependence on lighting conditions, the need for a front-facing camera, limited field-of-view, and high processing requirements (Alvarez et al, 2016).

Roberts et al (2012) proposed Infra-Red (IR) sensors. If arranged in an array, these enables an accurate measure or relative bearing between two MAVs. Unfortunately, because IR is uni-directional, several sensors are needed to each face in a direction. This is not easily exportable to smaller MAVs.

Alternatively, recent work by Basiri (2015) uses on-board sound-based localization. A microphone array and a chirp generator are mounted on-board of the MAVs, and the difference between arrival times of the chirp at the different microphones is used to estimate the relative bearing (Basiri et al, 2014, 2016). This method requires dedicated hardware, which for smaller MAVs can account for an increase in mass of even 10%-20% (Basiri et al, 2016; Remes et al, 2014).

To truly minimize the footprint, we decide to focus on a component that is mounted by necessity on all MAVs: a wireless transceiver. This is typically used for communication with a ground station (Lehnert and Corke, 2013; McGuire et al, 2016), but it may also be used for intra-swarm

communication. The signal strength of a wireless communication decreases with distance from the antenna, and can be used as a measure for range between MAVs. Szabo (2015) first exploited this on-board of real MAVs as a measure for range sensing. However, range-only data, coupled with significant noise and disturbances, were found insufficient to guarantee safe flight of two or more MAVs in a confined area in spite of relying on a complex evolved avoidance behavior. Amrita and Kumar (2016) recently also explored range-only avoidance on WeBot robots (in simulation only), but range measurements were aided by an array of proximity sensors.

Transceivers can be exploited for both ranging and data-exchange. Based on this, we developed a fusion filter that can determine relative location estimates via communicating on-board states between MAVs. To the best of our knowledge, the only instance of on-board relative localization using a wireless transceiver was recently brought forward by Guo et al (2016a) with Ultra Wide-Band (UWB) technology. However, they make use of one of the MAVs as a static beacon and their method relies on highly accurate distance measurements. Instead, we propose a method that complements possibly noisy distance measurements by communicating on-board states between *moving* MAVs. We then show how it can be used for indoor collision avoidance. We extensively validate this on real platforms as light as 50g that communicate between each other using Bluetooth, which is highly prone to noise and disturbances.

3 Communication-Based Relative Localization

Relative localization is achieved via wireless communication link between the MAVs. The idea is that the MAVs communicate the following states to each-other: planar velocity in the body frame, orientation with respect to North, and height from the ground. When communicating, the MAVs can also capture the strength of the signal, which acts as a measure of distance. For Bluetooth Low Energy (BLE), the technology chosen in our implementation, signal-strength measurements are referred to as Received Signal Strength Indication (RSSI). Each MAV fuses the received states, the RSSI, and its own on-board states to estimate the relative pose of another MAV. When multiple MAVs are present, multiple instances of the fusion filter run in parallel so that each MAV may keep track of the others. This section details the design and implementation of the relative localization scheme and presents some preliminary localization results that were obtained in early stages of the research.

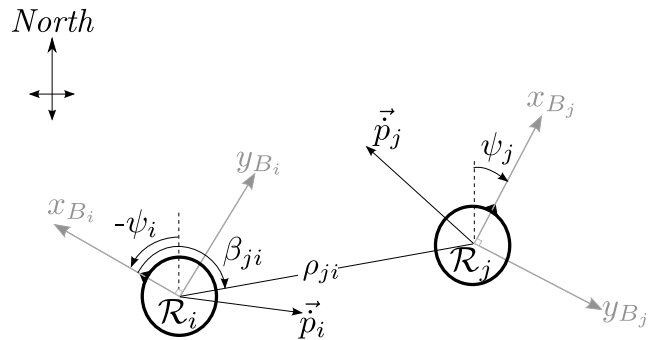


Fig. 1 Top view of the relative localization framework (x_B and y_B are the planar axis of \mathcal{F}_B , while z_B is positive downwards)

3.1 Framework Definition for Relative Localization

Consider two MAVs \mathcal{R}_i and \mathcal{R}_j with body-fixed frames \mathcal{F}_{B_i} and \mathcal{F}_{B_j} , respectively. We define the relative pose of \mathcal{R}_j with respect to \mathcal{R}_i as the set $\mathbf{P}_{ji} = [\rho_{ji}, \beta_{ji}, z_{ji}, \psi_{ji}]$, where ρ_{ji} represents the range between the origins of \mathcal{F}_{B_i} and \mathcal{F}_{B_j} , β_{ji} is the horizontal planar bearing of the origin of \mathcal{F}_{B_j} with respect to \mathcal{F}_{B_i} , z_{ji} is the height of \mathcal{R}_j with respect to \mathcal{R}_i and ψ_{ji} is the yaw of \mathcal{F}_j with respect to \mathcal{F}_i . See Fig. 1 for an illustration. Note that ρ_{ji} and β_{ji} are related to their cartesian counterparts via:

$$\rho_{ji} = \sqrt{x_{ji}^2 + y_{ji}^2 + z_{ji}^2} \quad (1)$$

$$\beta_{ji} = \text{atan2}(y_{ji}, x_{ji}) \quad (2)$$

x_{ji} , y_{ji} , and z_{ji} are the Cartesian coordinates of the origin of \mathcal{R}_j in \mathcal{F}_{B_i} .

3.2 Signal Strength as a Range Measurement

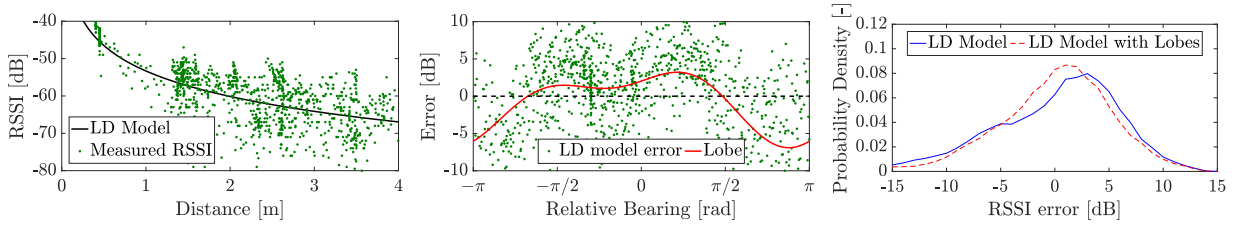
Let S_{ji} be the RSSI measurement in *dB*. It is correlated with ρ_{ji} by a function $\mathcal{L}(\rho_{ji})$. We define this function based on the Log-Distance (LD) model (Seybold, 2005):

$$S_{ji} = \mathcal{L}(\rho_{ji}) = P_n - 10 \cdot \gamma \cdot \log_{10}(\rho_{ji}). \quad (3)$$

P_n is the RSSI at a nominal distance of 1m. γ is the *space-loss parameter*, which dictates how much the signal strength decays with distance (for free-space: $\gamma = 2.0$).¹ The LD model is assumed subject to Gaussian noise (Svečko et al, 2015).

In preliminary tests, we analyzed the LD model with Ladybird MAV (Remes et al, 2014) connected via Bluetooth

¹ Experimentally, it has been found that office buildings can feature $2 \leq \gamma \leq 6$ (Kushki et al, 2008). Performing a sensitivity analysis of the LD model shows that an accurate identification of γ has a low impact on the distance estimate at small distances.



(a) RSSI measurements with respect to distance (green-dotted) and fitted LD model (black, solid) **(b)** Error about LD model with respect to relative bearing (green, dotted) fitted with a second order Fourier series (red, solid) **(c)** Noise distribution about the LD model without (blue, solid) and with (red, dashed) lobe effects

Fig. 2 Results of RSSI measurements during an experiment whereby a Ladybird MAV was carried in circles around a fixed Bluetooth antenna

to a fixed W1049B omni-directional antenna (Pulse, 2008). The MAV was carried in concentric circles at different distances around the antenna whilst RSSI was being recorded with the antenna. Its orientation with respect to North was kept constant, thus varying the relative bearing to the antenna. Ground-Truth (GT) data was recorded with an Optitrack Motion Capture System (MCS). The results from a representative data-sample are shown in Fig. 2, to which the LD model was fitted using a non-linear Least Squares (LS) estimator as in Fig. 2a. Among a set of similar experiments, the Standard Deviation (SD) of the error about the fitted LD model was found to be between $3dB$ and $6dB$. This is in line with literature (Szabo, 2015; Nguyen and Luo, 2013).

We also observed a change of the error with the relative bearing. This is shown in Fig. 2b, and accounts for the skew in error distributions, see Fig. 2c. The disturbances that can cause this were found to be: propagation lobes, interference by the reflection of the signal in the environment, the presence of other signals in the $2.4GHz$ spectrum, or other objects that obstruct the signal (Seybold, 2005; Svečko et al, 2015; Szabo, 2015; Kushki et al, 2008; Caron et al, 2008). The LD model could be expanded with this, but the susceptibility to environmental disturbances would lead to a confounding element between bearing and range which could be detrimental to the convergence of the fusion filter.

3.3 Localization via Fusion of Range and On-board States

Achieving a relative pose estimate requires measuring or inferring all four variables in \mathbf{p}_{ji} . From those, we can directly measure or observe the following three:

- ρ_{ji} : (range), available via RSSI as in Sect. 3.2.
- z_{ji} (relative height): Each MAV is expected to measure its height above the ground. This could be done with a pressure sensor (Beard, 2007; Sabatini and Genovese, 2013; Shilov, 2014), sonar, or a downward-facing camera (Kendoul et al, 2009b,a). Two MAVs \mathcal{R}_i and \mathcal{R}_j can share their altitude data, such that: $z_{ji} = z_j - z_i$.

- Ψ_{ji} (relative orientation): It is assumed that all MAVs acknowledge a common planar axis, e.g. magnetic North (No et al, 2015; Afzal et al, 2011). Via communication, the MAVs can share their orientation data.

Relative bearing is the only unknown variable. It becomes observable when fusing the three measurements above with velocity measurements, as shown in Martinelli and Siegwart (2005) and Martinelli et al (2005). We chose to perform sensor fusion with a discrete-time Extended Kalman Filter (EKF) due to its efficient processing and memory requirements (De Silva et al, 2014). The state transition model from time step k to $k+1$ was defined as in Eq. 4:

$$\begin{bmatrix} \mathbf{p}_{ji} \\ \dot{\mathbf{p}}_i \\ \dot{\mathbf{p}}_{jRi} \\ \Psi_j \\ \Psi_i \\ z_j \\ z_i \end{bmatrix}_{k+1} = \begin{bmatrix} \mathbf{p}_{ji} + (\dot{\mathbf{p}}_{jRi} - \dot{\mathbf{p}}_i) \Delta t \\ \dot{\mathbf{p}}_i \\ \dot{\mathbf{p}}_{jRi} \\ \Psi_j \\ \Psi_i \\ z_j \\ z_i \end{bmatrix}_k + \mathbf{v}_k \quad (4)$$

$\mathbf{p}_{ji} = [x_{ji} \ y_{ji}]^T$ holds Cartesian equivalents of bearing and range. $\dot{\mathbf{p}}_i = [\dot{x}_i \ \dot{y}_i]^T$ is a vector of the velocity of \mathcal{R}_i in \mathcal{F}_{B_i} (see Fig. 1). $\dot{\mathbf{p}}_{jRi}$ is $\dot{\mathbf{p}}_j$ rotated from \mathcal{F}_{B_j} to \mathcal{F}_{B_i} . Δt is a discrete time step between updates equal to the time between k and $k+1$. \mathbf{v}_k represents the noise in the process at time step k . This model assumes that all current velocities and orientations remain constant between time-steps. The observation model for the EKF is given by Eq. 5.

$$\begin{bmatrix} S_{ji} \\ \dot{\mathbf{p}}_i \\ \dot{\mathbf{p}}_j \\ \Psi_j \\ \Psi_i \\ z_j \\ z_i \end{bmatrix}_k = \begin{bmatrix} \mathcal{L}(\rho_{ji}) \\ \dot{\mathbf{p}}_i \\ \mathbf{R}_{2D}(\Psi_{ji}) \cdot \dot{\mathbf{p}}_{jRi} \\ \Psi_j \\ \Psi_i \\ z_j \\ z_i \end{bmatrix}_k + \mathbf{w}_k \quad (5)$$

$\mathbf{R}_{2D}(\cdot)$ is a 2D rotation matrix that uses the relative heading Ψ_{ji} to rotate the state estimate $\dot{\mathbf{p}}_{jRi}$ from \mathcal{F}_{B_i} to \mathcal{F}_{B_j} .

\mathbf{w}_k represents the noise in the measurements at time step k . Note that ρ_{ji} is expanded as per Eq. 1 so as to observe x_{ji} and y_{ji} .

The EKF cannot be initialized with a correct relative localization estimate, since this is not known; it must converge towards the correct estimate during flight. Appropriate tuning of the EKF noise covariance matrices is key to achieving this. In the EKF, the measurement noise matrix \mathbf{R} is a diagonal matrix with the form shown in Eq. 6.

$$\mathbf{R} = \begin{bmatrix} \sigma_m^2 & & & \\ & \sigma_v^2 \cdot \mathbf{I}_{4 \times 4} & & \\ & & \sigma_\psi^2 \cdot \mathbf{I}_{2 \times 2} & \\ & & & \sigma_z^2 \cdot \mathbf{I}_{2 \times 2} \end{bmatrix}. \quad (6)$$

σ_m is the assumed SD of S_{ji} . σ_v is the assumed SD of $\dot{\mathbf{p}}_i$ and $\dot{\mathbf{p}}_j$. σ_ψ is the assumed SD of the magnetic orientation measurements. σ_z is the assumed SD of the height measurements. $\mathbf{I}_{n \times n}$ is a $n \times n$ identity matrix. Based on our preliminary RSSI noise analysis, σ_m is tuned to $5dB$. All other SDs were tuned to 0.2, unless otherwise stated.

The process noise matrix \mathbf{Q} is the diagonal matrix presented in Eq. 7.

$$\mathbf{Q} = \begin{bmatrix} \sigma_{Q_p}^2 \cdot \mathbf{I}_{2 \times 2} & & & \\ & \sigma_{Q_v}^2 \cdot \mathbf{I}_{4 \times 4} & & \\ & & \sigma_{Q_\psi}^2 \cdot \mathbf{I}_{2 \times 2} & \\ & & & \sigma_{Q_z}^2 \cdot \mathbf{I}_{2 \times 2} \end{bmatrix}. \quad (7)$$

σ_{Q_p} is the SD of the process noise on the relative position update. σ_{Q_v} , σ_{Q_ψ} , and σ_{Q_z} are SDs for the expected updates in velocity, orientation, and height respectively. The tuning of \mathbf{Q} defines the validity of the process equations (Malyavej et al, 2013). The tuning is made such that a *high-level of trust is put on the relative position update*. This approach is key to encouraging convergence and helps to discard the high noise and disturbance in the RSSI measurements. Unless otherwise stated: $\sigma_{Q_p} = 0.1$, while $\sigma_{Q_v} = \sigma_{Q_\psi} = \sigma_{Q_z} = 0.5$.

The filter is limited by *flip and rotation ambiguity* as defined in (Cornejo and Nagpal, 2015). When the motion of \mathcal{R}_j perfectly matches the motion by \mathcal{R}_i , range-only measurements remain constant and are not informative for bearing estimation. If the MAVs do not fly in formation, the probability of this event is low (Cornejo and Nagpal, 2015). The same ambiguity takes place when both \mathcal{R}_i and \mathcal{R}_j are static; motion by at least one MAV is required.

3.4 Implementation Details

We used BLE to enable communication between the MAVs. The data is sent and received by means of advertising messages scheduled using a Self-Organized Time Division Multiple Access (STDMA) algorithm (Gaugel et al, 2013). This

way, each MAV's Bluetooth antenna alternates between advertising and listening. This enables direct communication and circumvents the Master-Slave paradigm otherwise enforced by the Bluetooth standard (Townsend et al, 2014). The message rate is $5Hz$, i.e. data is received every $0.2s$.

3.5 Preliminary Relative Localization Tests

We performed preliminary localization tests with a Ladybird MAV around a fixed Bluetooth W1049B antenna. The objective was to determine how well the antenna could localize the MAV. An Optitrack MCS was used to guide the MAV in circular flights and record its GT velocity, orientation, and height. The antenna measured the RSSI with the MAV. The recorded GT data was altered with Gaussian noise with $\sigma_v = 0.2m/s$, $\sigma_z = 0.2m$, and $\sigma_\psi = 0.2rad$, and then used as measurements for the EKF. In the LD model of the EKF: $P_n = -63dB$ and $\gamma_l = 2.0$. The EKF was initialized with a null guess position of $x_{ji} = y_{ji} = 1m$. In these preliminary tests, the localization filter was applied off-board.

Fig. 3 shows the results. Estimates for x_{ji} and y_{ji} are shown in Fig. 3a and Fig. 3b, the EKF converges towards GT in the first few seconds, after which it tracks successfully. Fig. 3c shows the estimated range, where we can observe a significant improvement in error with respect to an inverted LD model. Note that the range error increases with distance, this is due to the logarithmic nature of RSSI propagation. Fig. 3d shows the bearing error, which is small throughout most of the flight. The only exceptions are occasional spikes which occur at small distances which cross over $x_{ji} = 0m$ and $y_{ji} = 0m$. This is because at very small distances, a small error in x_{ji} or y_{ji} can translate into a significant error in β_{ji} . Thanks to the avoidance algorithm, such small distances should be avoided altogether during flights.

4 Collision Avoidance Behavior

The avoidance algorithm was inspired by the Collision Cone (CC) frame-work as seen in the works by Fiorini and Shiller (1998) and Wilkie et al (2009). A collision cone is a set of all velocities of an agent that are expected to lead to a collision with an obstacle at a given point in time. Its name is derived from the fact that it is geometrically cone-shaped. This section details our implementation of collision cones and how it is used to determine an avoidance trajectory.

4.1 Collision Cones and Avoidance Strategy

Take two MAVs \mathcal{R}_i and \mathcal{R}_j . The collision cone CC_{ji} (depicted in Fig. 4) would include all velocities of \mathcal{R}_i which

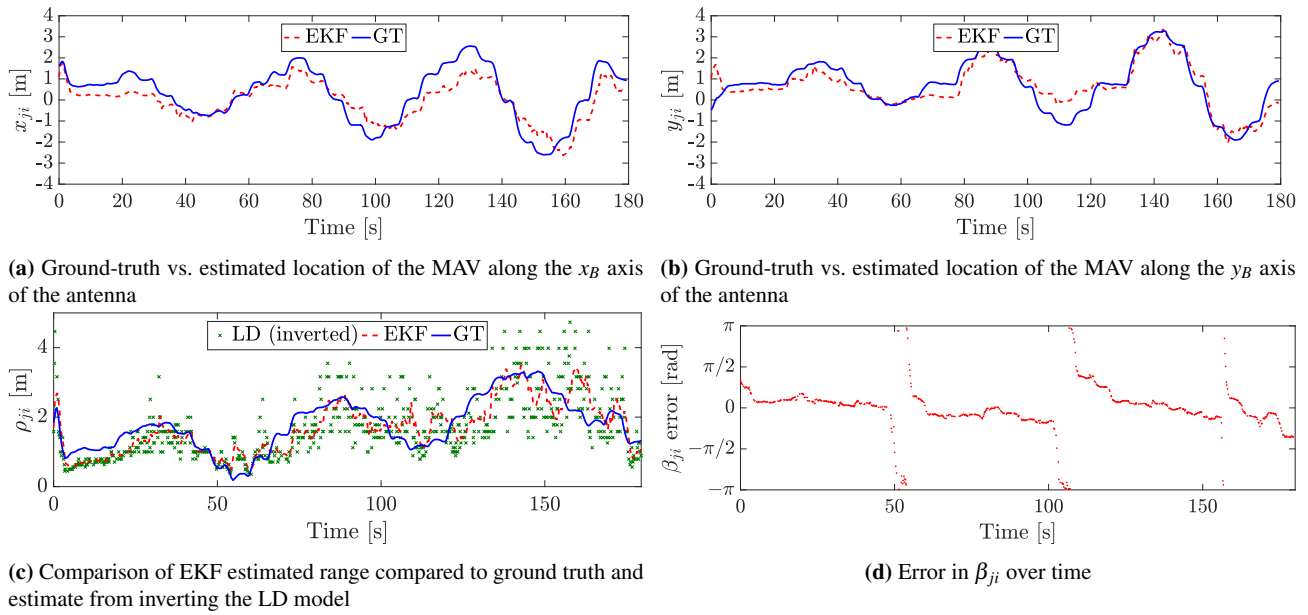


Fig. 3 Preliminary localization results based on circular flights of a Ladybird MAV around a fixed antenna (averaged over 50 iterations of artificial noise added to the velocity, height, and orientation measurements)

could lead to a collision with \mathcal{R}_j . It is constructed in three steps.

1. A cone CC_{ji} is defined as in Eq. 8. α is an arbitrary angle. x and y are points on x_{B_i} and y_{B_i} , respectively. The cone is characterized by an expansion angle $\alpha_{CC_{ji}}$, subject to $0 < \alpha_{CC_{ji}} < \pi$.

$$CC_{ji} = \left\{ (x, y) \in \mathbb{R}^2; \alpha \in \mathbb{R}; |\alpha| \leq \frac{|\alpha_{CC_{ji}}|}{2} : \tan(\alpha)x = y \right\} \quad (8)$$

2. CC_{ji} is rotated so as to be centered around the estimated bearing to the obstacle \mathcal{R}_j as in Eq. 9, where: $\bar{\beta}_{ji}$ is the estimated β_{ji} from the EKF, \leftarrow is an update operator, and $\mathbf{R}(\cdot)$ is a rotation operator for the set.

$$CC_{ji} \leftarrow (\mathbf{R}(\bar{\beta}_{ji}) \cdot CC_{ji}) \quad (9)$$

3. The cone is translated by the estimated velocity of \mathcal{R}_j expressed in \mathcal{F}_{B_i} , to account for the fact that the obstacle is moving, as per Eq. 10. $\bar{\mathbf{p}}_{jRi}$ is the estimated \mathbf{p}_{jRi} from the EKF. The operator \oplus denotes the translation of a set by a vector.

$$CC_{ji} \leftarrow CC_{ji} \oplus \bar{\mathbf{p}}_{jRi} \quad (10)$$

In a team of m MAVs, each member \mathcal{R}_i holds $m - 1$ collision cones that it can superimpose into a single set CC_i :

$$CC_i = \bigcup_{j=1}^{m-1} CC_{ji} \quad (11)$$

If, during flight, $\dot{\mathbf{p}}_i \in CC_i$, then a *clock-wise search* about the z_{B_i} axis (starting with the current desired velocity) is used to determine the desired escape velocity. If no solution is found, then the search is repeated for a higher escape speed.

The clock-wise search encourages a preference for right-sided maneuvers with respect to the current flight direction. This differentiates it from the Velocity Obstacle (VO) avoidance method, which selects a flight direction that minimizes the required change in velocity. This automatically resolves an issue known as “reciprocal dances”, which are left-right dances when two entities heading towards each-other repeatedly select the same escape direction. Other solutions to reciprocal dances assume reciprocity, meaning the assumption that the other member will also take a certain evasive action (Snape et al, 2009, 2011; Van Den Berg et al, 2011). In our case, however, due to the potential for large relative localization errors, MAVs cannot safely assume that the others will participate in a suitable and reciprocal escape maneuver.

4.2 Tuning the Expansion Angle of the Collision Cone

The expansion angle of a collision cone is dependent on the distance between the MAVs (the MAV radii becomes more significant as distance decreases), and the relative estimation errors (Conroy et al, 2014). Based on this knowledge, we formulated (12) to calculate the expansion angle:

$$\alpha_{CC_{ji}} = 2 \cdot \tan^{-1} \left(\frac{2r + \bar{\rho}_{ji} + \varepsilon_\alpha}{\kappa_\alpha \cdot \bar{\rho}_{ji}} \right), \quad (12)$$

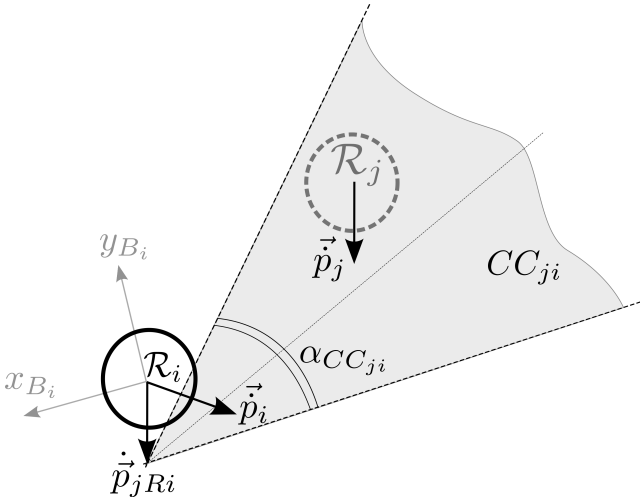


Fig. 4 Depiction of CC_{ji} that \mathcal{R}_i holds with respect to the estimated location of \mathcal{R}_j

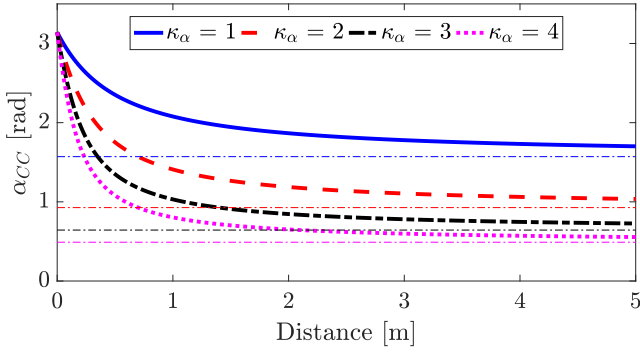


Fig. 5 Effect of κ_α on $\alpha_{CC_{asymptote}}$ ($r = 0.1m$, $\varepsilon = 0.5$)

where: r is the radius of a MAV (modeled as a circle); \bar{p}_{ji} is the estimated range between \mathcal{R}_i and \mathcal{R}_j ; ε_α is an additional margin, the properties of which are discussed in Sect. 4.3; and κ_α is a coefficient describing the quality of the estimate. The expansion has a lower bound $\alpha_{CC_{asymptote}}$ which is dependent on κ_α :

$$\alpha_{CC_{asymptote}} = \lim_{\bar{p}_{ji} \rightarrow \infty} \alpha_{CC_{ji}} = 2 \cdot \tan^{-1} \left(\frac{1}{\kappa_\alpha} \right). \quad (13)$$

Its impact may be appreciated in Fig. 5. In this work, unless otherwise stated, we use $\kappa_\alpha = 1$, leading to $\alpha_{CC_{asymptote}} = \frac{\pi}{2}$. This incorporates the expected bearing errors expected during flight based on our preliminary results.

4.3 Preserving Behavior in Rooms of Different Size

The expansion angle of the collision cone widens towards π as the distance between two MAVs decreases. This implies that in smaller rooms, the collision cones will *always*

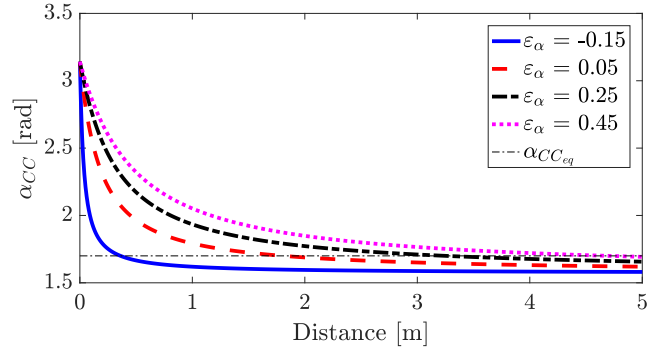


Fig. 6 Effect of ε_α on α_{CC} ($r = 0.1m$, $\kappa_\alpha = 1$)

feature wide expansion angles, leading to most of the environment becoming out of bounds. This restriction in freedom of movement creates oscillations in MAV trajectories. To solve the issue, we propose using the margin ε_α as a tuning parameter. The effect of varying ε_α may be appreciated with Fig. 6: as ε_α decreases, the decay of the expansion angle with distance increases. A faster decay is suitable for smaller rooms so that motion is less restricted.

We devised a method to tune ε_α intuitively. By re-arranging Eq. 12, ε_α is expressed by:

$$\varepsilon_\alpha = \kappa_\alpha \cdot \rho_{eq} \cdot \tan \left(\frac{\alpha_{CC_{eq}}}{2} \right) - 2r - \rho_{eq}, \quad (14)$$

This translates tuning ε_α to tuning a pair $\{\rho_{eq}, \alpha_{CC_{eq}}\}$, where $\alpha_{CC_{eq}}$ is the desired angle of expansion at a distance ρ_{eq} . Note that $\alpha_{CC_{eq}} > \alpha_{CC_{asymptote}}$, and $\varepsilon_\alpha \geq -(r_i + r_j)$ if $\kappa_\alpha \geq 1$. In all our tests, ρ_{eq} is set to half of the side length of the room. $\alpha_{CC_{eq}}$ is kept at $1.7rad$.

5 General Testing Methodology

5.1 Description of Arbitrary Task for Performance Testing

A test exploration task was developed where multiple MAVs fly in a room, at the same altitude, and attempt to pass *through* the center. This is designed to provoke collision and observe if/how they are resolved. Consider a team of m homogeneous MAVs. Each MAV \mathcal{R}_i can control its velocity. Let $\dot{\mathbf{p}}_{i_{cmd,k}}$ be the desired velocity for \mathcal{R}_i expressed in its body-frame \mathcal{F}_{B_i} at a given time-step k . Let d_{wall_i} be the distance between \mathcal{R}_i and the arena border that is closest to it, with d_{safe} being a safety distance to the arena's borders. Remember that each robot \mathcal{R}_i features $m - 1$ EKF instances to keep track of the other members and uses their outputs to determine its collision cone set CC_i , see Eq. 11. At each-time step k , the EKF outputs are updated and CC_i is re-calculated. $\dot{\mathbf{p}}_{i_{cmd,k}}$ is then chosen as follows: $\dot{\mathbf{p}}_{i_{cmd,k}} = \dot{\mathbf{p}}_{i_{cmd,k-1}}$ unless conditions M1 and M2 take place.

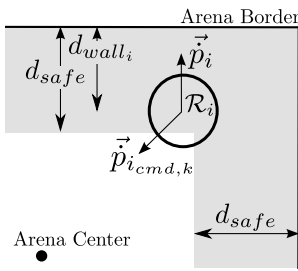


Fig. 7 Depiction of condition M1

M1: $d_{wall_i} < d_{safe}$ and $\dot{d}_{wall_i} < 0$. This means that \mathcal{R}_i is close to the arena border and approaching it. Then, $\dot{\mathbf{p}}_{i_{cmd,k}}$ is rotated towards the center of the arena. See Fig. 7.

M2: $\dot{\mathbf{p}}_i \in CC_i$. This means that the current velocity of \mathcal{R}_i could lead to a collision with one or more team members. An escape velocity is sought according to the strategy proposed in Sect. 4.

Condition M1 holds priority over M2 to ensure that the MAVs remain within the arena. At all time-steps, unless otherwise commanded by the collision avoidance algorithm, $|\dot{\mathbf{p}}_{i_{cmd,k}}| = v_{nominal}$, where $v_{nominal}$ is a fixed speed magnitude.

5.2 Assessment Strategy

Assessment of Relative Localization: During the task, this can be assessed by comparing the estimated relative locations to ground-truth data.

Assessment of Collision Avoidance: This is partially dependent on the performance of the relative localization, yet can be assessed independently by identifying failure cases and observing general behavior properties. It is also interesting to determine the likelihood that the error falls within the expected collision cone bounds.

Assessment of the Full System: The parameter of interest is the mean flight-time between collision. Ideally, a successful system is one that systematically ensures that collision will not take place. This metric is dependent on how crowded the airspace is. By modeling MAVs as circles, airspace density is calculated with:

$$\mathcal{D}_{m,c} = \frac{m \cdot \pi r_c^2}{s_c^2} \quad (15)$$

$\mathcal{D}_{m,c}$ denotes the density for configuration c with m MAVs. r_c is the radius of a MAV in configuration c . s_c is the side length of the squared arena at configuration c .

Experiments were performed in separate stages with increasing realism and autonomy, starting with simulation and ending with autonomously controlled flight with on-board measurements. After this, the technology was also ported

and tested on miniature drones. The results of all tests are discussed in the next four chapters. Videos of the experiments are available at: https://www.youtube.com/playlist?list=PL_KSX9G0n2P9f0qyWQNBmj7xpe1HARSpC.

6 Simulation Experiments

Simulations allow to assess the collision avoidance algorithm and the full system. We can easily assess the performance of the system for several airspace densities, noise scenarios, etc., and obtain statistically relevant insights.

6.1 Simulation Environment Set-Up

The simulation environment was developed using Robotics Operating System (ROS) (Quigley et al, 2009), the Gazebo physics engine (Koenig and Howard, 2004) and the hector-quadrotor model (Meyer et al, 2012). Multiple quad-rotor MAVs can be simulated simultaneously. A ROS module (or “node”) for each MAV simulates the Bluetooth communication and enforces the controller described in Sect. 5.1. A rendered screen-shot of a simulation run is shown in Fig. 8a.

The RSSI is simulated using the LD model ($P_n = -63dB$, $\gamma_l = 2.0$) with added Gaussian noise (SD of 5db) and horizontal antenna lobes, unless otherwise stated. The lobes were modeled using a third order Fourier series with unitary weights, see Fig. 8b. The other measurements were altered with the same standard deviations as in the preliminary localization tests of Sect. 3.5. Furthermore: $v_{nominal} = 0.5m/s$, $d_{safe} = 0.25m$, and $\Psi = 0rad$ for all MAVs. The MAVs begin at different corners of the arena. The EKF is initialized such that the initial position guess is towards their initial flight direction (i.e. the center of the arena).

We investigated twelve combinations of arena size and MAV diameter for teams of two MAVs and three MAVs. The combinations will be referred to by the encircled numbers in Fig. 9. Each configuration was simulated 100 times. Each simulations was automatically interrupted if a collision occurred, or after 500s of collision-free flight.

6.2 Results

Mean time-of-flight for each configuration is shown in Fig. 10. Flights with three MAVs consistently show a lower performance than with two MAVs. The performance drop is a result of the team dynamics at play, namely: 1) increased airspace density; 2) decreased freedom of movement due to superposition of collision cones. These two factors are analyzed in the remainder of this section.

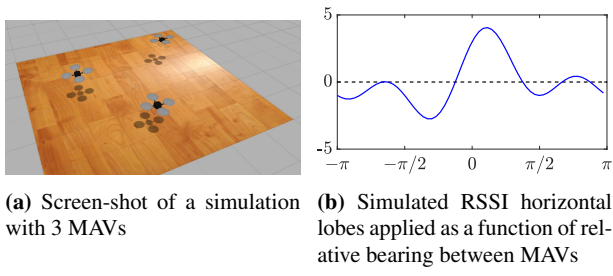


Fig. 8 Figures relating to the development of the simulation environment

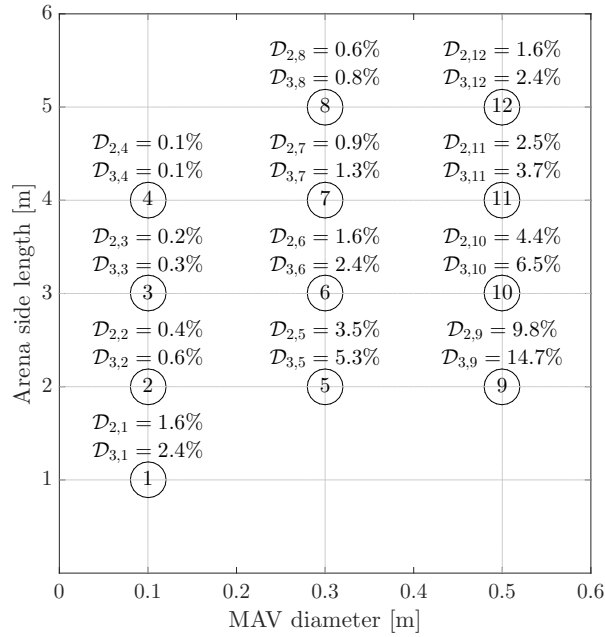


Fig. 9 The twelve configurations tested in simulation with configuration numbers shown in the white circles

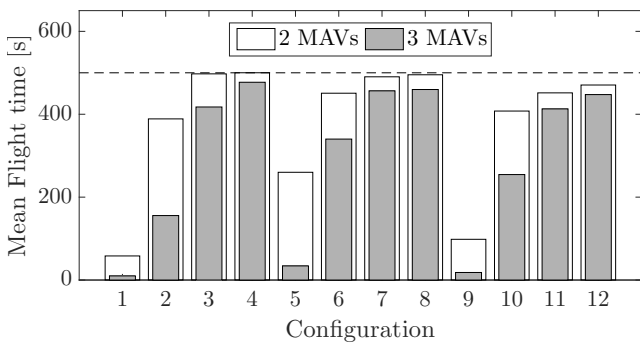
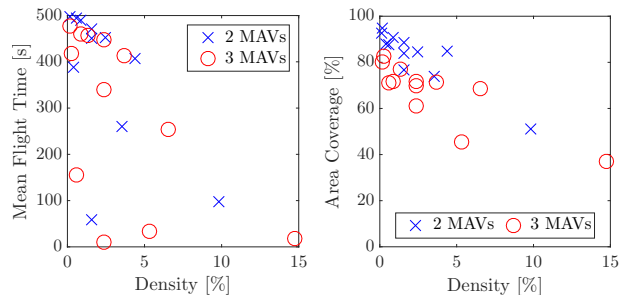


Fig. 10 Mean flight-time to collision for all simulated configurations. Average results without collision avoidance, not shown in this figure, range between 3.9s and 14.3s.

When the arena side-length remains constant and the MAV diameter increases, a decrease in mean flight-time is observed. This is seen by comparing within the configura-



(a) Mean flight-time with respect to density (b) Mean area-coverage with respect to density

Fig. 11 Flight parameters with respect to airspace density based on simulation results

tion triads 4-7-11, 3-6-10, and 2-5-9, and the pair 8-12. The result is analogous when MAVs of the same diameter are used in arenas of different sizes, see the configuration quartets 1-2-3-4, 5-6-7-8, and 9-10-11-12. This implies that a lower density improves the probability of success, but this is found to not strictly be the case. Fig. 11a shows the flight time to collision as a function of the airspace density. A portion of configurations show low results in spite of the low airspace density, and are outliers in the negative linear trend. These correspond to configurations 1, 2, 5, and 9, which feature smaller arena sizes. The conclusion is that room size affects performance even when airspace density remains constant. This is a remaining limitation of the current status of the system when operating in smaller room sizes. Its causes are discussed in Sect. 10.2.

Fig. 11b shows the impact of airspace density on area coverage for all flights with two MAVs and three MAVs. Area coverage was measured as follows. The total area is divided in sections of $0.20m \times 0.20m$. A section is marked “covered” when one of the MAVs crosses it during a trial. Area coverage is the percentage of covered sections. With this, two patterns arise.

1. A higher airspace density leads to a lower overall coverage. This is due to: a) lower flight times, providing less overall time to complete the mission, and b) decreased freedom of movement due to larger portions of the arena being covered by collision cones.
2. Three MAVs systematically achieve lower area coverage than only two MAVs in the same configuration. This is explained by analyzing the flight trajectories in more detail, from which an emergent circular behavior is discerned. See, for instance, Fig. 12, which shows two exemplary runs from a simulation with two (Fig. 12a) and three (Fig. 12b) MAVs from configuration 10. When more than one MAV to avoid is present, the superposition of multiple collision cones significantly discourages the pursuit of the desired trajectory. The result is clock-wise

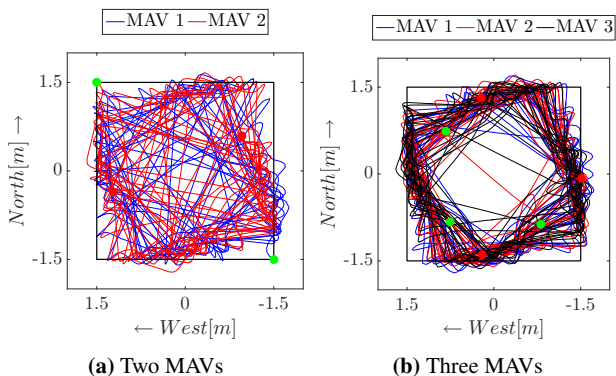


Fig. 12 Emergent circular behavior from two exemplary flights of 500s extracted from configuration 10 (green = starting position, red = final position)

motion along the sides of the arena for all MAVs. Oscillations along the border are observed as conditions M1 and M2 alternate.

6.3 Impact of RSSI Noise on Performance

In simulation, two further case-studies were explored. In the first case, the simulated RSSI noise is reduced from 5dB to 3dB, but lobes are still simulated. In the second case, RSSI noise is kept at 5dB but sensor lobes are removed. All other parameters remain the same as in the primary simulations. The configurations tested are those with the lowest performance: 1, 2, 5, 6, 9, 10. The results are shown in Fig. 13, and show that removing the antenna lobes provides the largest improvement in performance. A lower noise also improves results, yet the impact is generally lower than antenna lobes. The lower error in relative position estimates translates to a more successful collision avoidance system. This implies that performance could be improved further if operating in cleaner environments, if using better antennas, or with a better filtering of noises.

7 Experiments featuring External Own-State Measurements

These experiments use Optitrack to accurately inform MAVs of their velocity, orientation, and altitude. This isolates the impact of using real RSSI measurements and Bluetooth communication on the relative localization system during flight. It also provides system performance data in the case of high-quality on-board estimates.

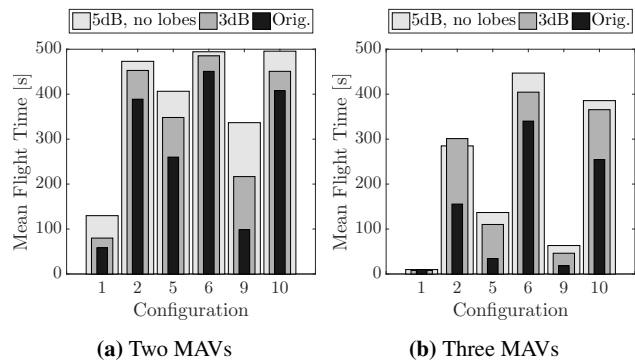


Fig. 13 Improvements in system performance against nominal results (“Orig.”, black, narrowest) when noise is reduced from 5dB to 3dB (dark gray, mid width) or when lobes are removed (dark gray, widest)



Fig. 14 A flight with 3 AR.Drones (encircled in white)

7.1 Experimental Set-Up

These experiments were performed using AR.Drones 2.0 (Parrot, 2012). A BLED112 (Labs, 2016) Bluetooth Smart USB Dongle enabled them with Bluetooth. The controller was developed using Paparazzi (Mueller and Drouin, 2007) and was running entirely on-board. The experiments in this section relied on Optitrack to provide each MAV with data of its own velocity, orientation, and height via a Wi-Fi link. Each AR.Drone then communicated this data via the Bluetooth broadcast to the other ones.

All MAVs flew at 1.5m from the ground, with a nominal speed $v_{nominal} = 0.5m/s$ and safety wall distance $d_{safe} = 0.5m$. The enforced arena size in all experiments was $4m \times 4m$, making these tests analogous to Configuration 11 from the simulation runs (AR.Drones are slightly larger in diameter than 0.5m). The LD model in the EKF filter was tuned with: $P_n = -68dB$ and $\gamma_l = 2.0$. P_n was obtained using a brief hand-held measurement, γ_l was based on the free-space assumption. The Optitrack measurements inputted into the EKFs were altered with Gaussian noises $\sigma_v = 0.2m/s$ and $\sigma_\psi = 0.2rad$. Fig. 14 shows a picture of a flight with 3 AR.Drones.

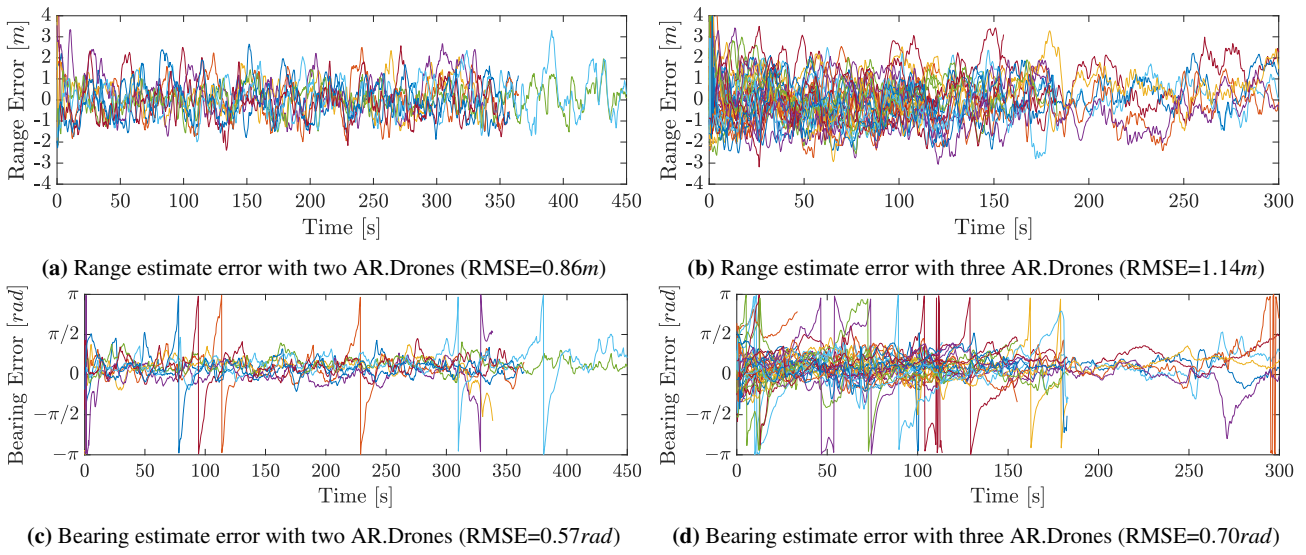


Fig. 15 Overview of all relative range (a,b) and relative bearing (c,d) estimation errors for flights with external state measurements

7.2 Results

Four flights were performed with two AR.Drones for a cumulative time of 25.3min. Only one collision took place, which occurred in the second flight after 5.6min. The other flights lasted 6.1min, 7.6min, and 6.0min without collisions; they were ended manually due to low battery.

Six controlled flights were performed with three AR.Drones for a cumulative time of 15.3min. Five flights ended in collisions. The flights ending with collisions reached featured a mean flight time of 160s (2.7min). The shortest flight was 33s, the longest was 5.2min. The other flights lasted 1.9min, 2.6min, and 3.0min. The flight without a collision was manually ended after 2.0min due to low battery. Overall, this set-up with three MAVs can expect a collision once every 184s ($\approx 3min$).

All relative localization range errors shown in Fig. 15a and Fig. 15b, and the bearing errors are shown Fig. 15c and Fig. 15d. The Root Mean Squared Error (RMSE) for flights with two MAVs is 0.57rad for bearing, and 0.86m for range. With three MAVs, the RMSE rises to 0.70rad and 1.14m, respectively. On occasion, we observe that the bearing error temporarily diverges towards $\pm\pi$. This error does not necessarily lead to collisions due to the non-reciprocal nature of the avoidance behavior. Nevertheless, it introduces a temporary uncertainty in the system. The error is more frequent with three AR.Drones. We also observe that the convergence rate for bearing estimates over flights with three AR.Drones is worse than with two AR.Drones. This may be appreciated in Fig. 16, zooming into the first 30s of Fig. 15c and

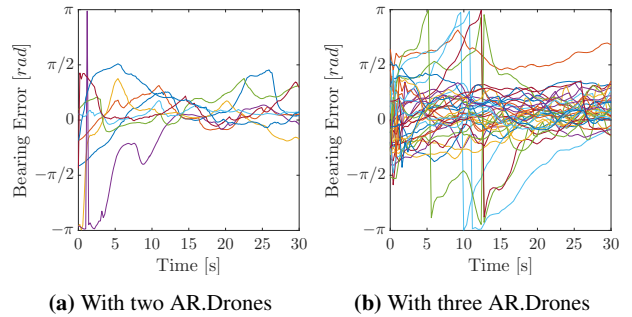


Fig. 16 Comparison of bearing estimate errors in the first 30 seconds of flight during flights with external state measurements

Fig. 15d in more detail. Convergence times for flights with three MAVs reach up to 30s prior to settling (Fig. 16b). By comparison, the convergence in flights with two AR.Drones only (Fig. 16a) is found to be at most within 5 – 10s.

8 Experiments featuring On-board Own-State Measurements

The experiments from the controlled flights were repeated but with on-board state estimation by the MAVs. Therefore, on-board MAV sensors measured and controlled velocity, orientation, and altitude. This shows real-world relative localization performance for collision avoidance.

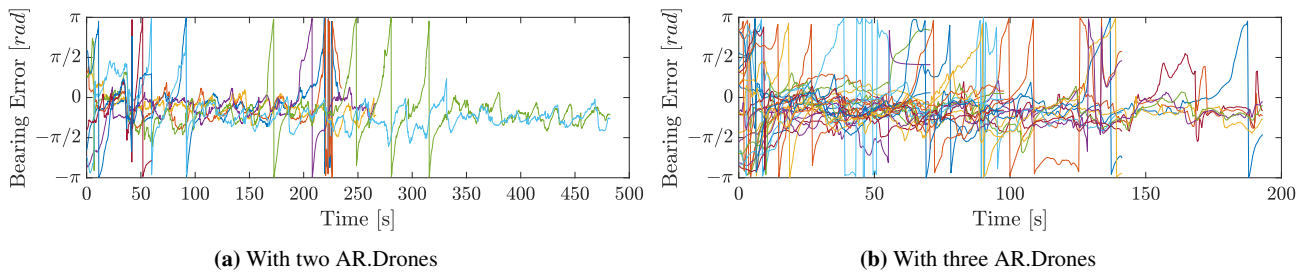


Fig. 17 Overview of relative bearing estimation errors for flights with two AR.Drones (a) and three AR.Drones (b) featuring on-board state estimation

8.1 Experimental Set-up

Velocity was estimated using the bottom facing camera and the *EdgeFlow* (McGuire et al, 2016). Orientation was measured using gyroscope integration (given an initial orientation towards North). Height from the ground was measured using sonar. Optitrack was *only* used to enforce condition M1 (wall detection), which featured $d_{safe} = 0.5$. This is because wall detection is outside of the purpose of this research. To further stress-test the system, a further change was that the EKFs initial relative position assumption was $x_{ji} = y_{ji} = 1m$ for any MAV \mathcal{R}_i with respect to any other \mathcal{R}_j , as opposed to the center of the arena. The AR.Drones communicated with a ground-station using a Wi-Fi link for logging and take-off/land control.

8.2 Results

Four flights were performed with two AR.Drones for a cumulative flight time of 17.3min. The flights lasted 3.9min, 4.4min, 8.0min, and 1.0min. Only the first and the last ended due to collisions. The second and third were ended due to low batteries. The third flight suffered from a near-collision in the early stages, but afterwards successfully continued until 8.0min without collisions. Another four flights were conducted with three AR.Drones, which lasted 8.3min cumulatively. The flights lasted 1.2min, 3.2min, 2.3min, 1.6min. The second flight was ended due to low batteries on one MAV. The other flights ended due to collisions between two of the three drones.

The bearing estimation error is shown in Fig. 17. The error has increased with comparison to the previous results. With two AR.Drones, the mean RMSE over the first three flights is 0.85rad. This is sufficient for a long collision-free flight time. In the last flight, however, the RMSE was 1.3rad, possibly due to a large disturbances in RSSI. This is eventually lead to a relatively early collision after 1.0min. With three drones, the bearing RMSE over all flights is 1.0rad. Furthermore, observing Fig. 17 we can note an accumulat-

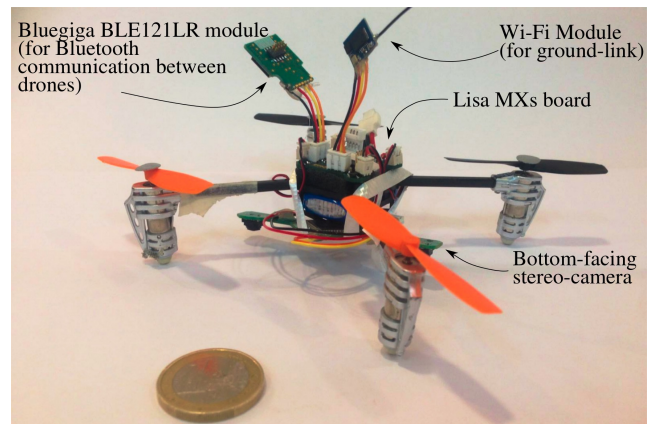


Fig. 18 Miniature drone used in the experiments

ing error bias in bearing over time due to the accumulating gyroscope bias. This should be corrected for future implementations by using the magnetometer to limit the accumulating bias.

9 Porting the technology to Miniature Drones

To show that the proposed solution scales to smaller MAVs, we ported the technology to Ladybird MAV. One test-ready MAV and its components are shown in Fig. 18. As for the AR.Drones, the Wi-Fi link was used for logging and take-off/land control.

9.1 Experimental Set-Up

A bottom facing camera and a gyroscope measured velocity and orientation, respectively. In the LD model, following a short hand-made calibration $P_n = -55dB$. Given the smaller size of the drones, the enforced flight arena was reduced to $2m \times 2m$ with $d_{safe} = 0.5m$. This scenario is similar to configuration 2 from Fig. 9. For simplicity, given the lack of a tested height sensor, height was controlled using Optitrack. The drones flew at slightly different heights to limit dam-

ages in case of failure by the collision avoidance system. All other test parameters stayed as for Sect. 8.

9.2 Results

Three flights were performed with this set up, lasting 2.8min, 3.7min, and 3.1min.² The first flight saw no collision cases. The second flight saw near collisions at 1.35min and at 3.7min. The latter came in light of low-batteries by one of the drones. As it lowered its height, the two MAVs also collided. The third flight saw a near collisions after $\approx 60s$ and ≈ 90 . Both took place in the corner when condition M1 takes over the drones, and are thus regarded more as a failure of the behavior than the relative localization. This shows the importance of implementing a method that keeps taking into account other drones while also avoiding the walls, which was not implemented in our controller.

It is noted that a slightly lower performance than previous experiments was expected due to the smaller arena size, an effect which was also observed in simulation and is discussed further in Sect. 10.2. Nevertheless, we also note a decrease in accuracy for relative localization as RMSE per flight ranges from 0.8rad to 1.37rad. Inspecting the data in more detail shows that this is the result of larger errors in both RSSI noise as well as lower quality on-board velocity estimates. The former is explained by the fact that the Bluetooth module was placed right next to the Wi-Fi module, creating disturbances.

10 Discussion

10.1 Performance of Relative Localization

In all AR.Drone tests, a noticeable loss in relative localization performance was measured when introducing a 3rd MAV. The effects were longer convergence times as well as higher relative bearing/range errors. A decrease in performance was also observed when using on-board velocity estimates. This was due to a combination of over-under estimation of velocity or occasional spikes in the measurements.

The relative localization scheme was implemented with an EKF. This may be criticized for its reliance on a Gaussian noise model. Robust (Kallapur et al, 2009) or adaptive (Sasiadek and Wang, 1999) variants of Kalman filters, or a Particle Filters (PFs) (Svečko et al, 2015), might be better

² The available flight footage shows how the MAVs avoided flying into each other for the duration of the flights. See https://www.youtube.com/playlist?list=PL_KSX9G0n2P9f0qyWQNBmj7xpe1HARSpc

suited to this end. However, a mere change in filter could increase computational costs without bringing a higher quality estimate. This is because there are a number of other limitations.

- The logarithmic decrease in RSSI makes it intrinsically insufficient to measure changes in range at larger distances. Without measurable changes in RSSI, bearing is no longer observable.
- RSSI disturbances in the environment cannot be fully modeled unless the environment is known a-priori.
- The proposed process update equation makes the null assumption that all velocities remain constant between time-steps. Improvements may come from including more complex dynamic properties in the process equation, e.g. acceleration and/or jerk.
- As seen throughout our tests, major improvements can come by improving the quality of on-board state estimates.

Further investigations are encouraged to define a filter that lowers the expected worst-case error.

Further improvements could also come from a change in communication hardware. In this work, we have achieved promising results using Bluetooth, which was selected due to its prompt availability on several drones. The noise and disturbances with Bluetooth, however, are large. Other hardware, such as UWB, would offer a significant reduction in noise, leading to better overall relative localization results. Based on our simulations from Sect. 6.3, this should automatically result in an improved overall system performance.

10.2 Performance of Collision Avoidance

In simulation, all twelve configurations have also been tested *without* active collision avoidance. The obtained mean flight times ranged between 3.9s and 14.3s. A z -test with 95% confidence level (Dekking, 2005) shows a statistically significant improvement in flight time for all configurations when using our method.

Fig. 11a showed that smaller rooms lead to poorer performance than larger rooms despite similar airspace density. The parameter ϵ_α , as explained in Sect. 4.3, implements room scaling within the collision cones. Reasons for this are:

- The ratio of arena size to $v_{nominal}$ decreases in smaller rooms.
- The communication rate is constant, which limits the decision rate of the collision avoidance controller.
- In smaller rooms, M1 is called more frequently, in which case collision cones are ignored according to the task in this article.

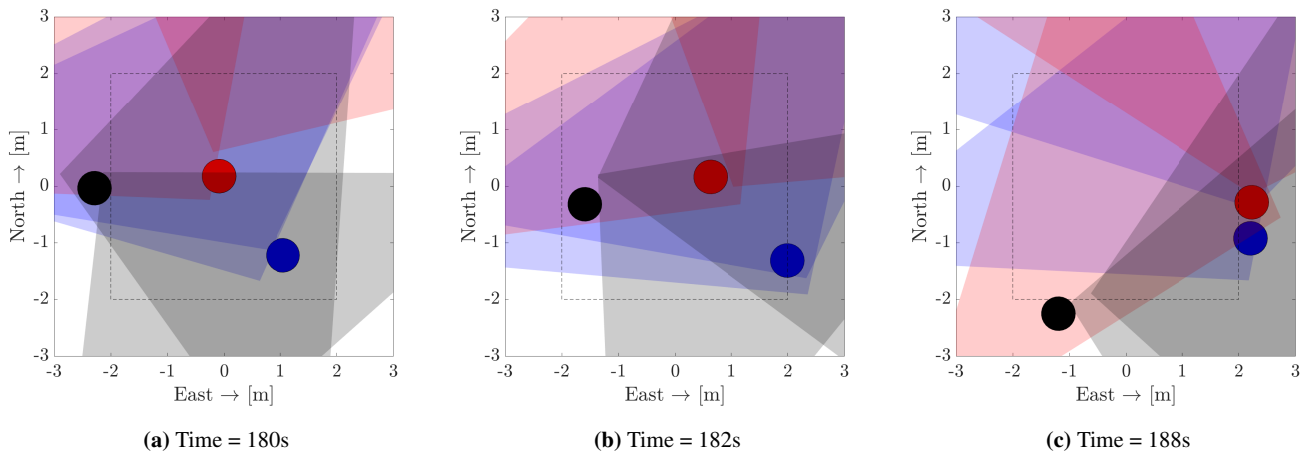


Fig. 19 Chronological depiction (left to right) of a collision case in a flight with 3 AR.Drones. Large circles indicate the ground-truth position in the arena, the triangles are the cones that each AR.Drone holds.

It was observed, and confirmed in simulation, that collisions for flights with three MAVs likely occur along the edges of the area. In the simulations of configuration 11, which is the one tested with the AR.Drones, 81% of the collided simulated flights with three MAVs ended within 0.5m of the arena borders. By comparison, only 35% of collisions with two MAVs occurred within this space. An example extracted from an AR.Drone flight recounted by the three events below (shown in Fig. 19).

1. One MAV is at the corner and reluctant to make movements towards the center. At time $t = 180s$ (Fig. 19a), we see this for the bottom right AR.Drone (blue). Its slow speed causes the red MAV to mistaken its estimate of the blue drone. In normal conditions, collision avoidance could still be achieved by the blue MAV, but it cannot react as it is trapped in the corner.
2. Another MAV turns towards the same side. In time $t = 182s$ (Fig. 19b), the central AR.Drone (red) avoids the black AR.Drone (on left) but in doing so goes to the right.
3. The second MAV also ends along the border and reluctant to make movements. At time $t = 188s$ (Fig. 19c), the two oscillate along the border until a collision occurs.

This scenario is less likely with two MAVs due to the larger freedom of movement and the higher relative localization accuracy. One method to limit this would be to reduce the angle of the collision cones for further-away MAVs, which increases mobility. Furthermore, it is also necessary to create an avoidance scheme that takes into account the wall and the drones together. This shall be tackled in future work.

11 Conclusion and Future Work

We have shown that it is possible to use wireless communication as a relative localization sensor that can be used on-board of MAVs operating in a team. This leads to a large reduction in collisions *without the need of a dedicated sensors*. With the solution proposed in this paper, a team of AR.Drones in a $4m \times 4m$ area could fly for several minutes without collisions. The technology was also used with miniature drones, showing its portability. With respect to the scenario in mind (i.e. the exploration of indoor spaces by MAV teams), this is an efficient method to limit collision risks in the event that MAVs end up flying in the same room.

The combined relative localization/collision avoidance system as presented and tested in this paper will be further improved in future work. Importantly, we will investigate UWB modules instead of a Bluetooth modules. Bluetooth suffers from high disturbances and noise that is detrimental to the performance, especially as more MAVs are introduced. Using UWB instead is expected to considerably improve the distance measurements used by the filter. Furthermore, the introduction of an avoidance strategy that makes a more informed decision near walls or when multiple MAVs are present is needed. This could resolve the more complex collision scenarios, especially in smaller rooms.

Videos

Videos of experiments are available at: https://www.youtube.com/playlist?list=PL_KSX9GOn2P9f0qyWQNBmj7xpe1HARSp.

A Bibliography

- Afzal MH, Renaudin V, Lachapelle G (2011) Magnetic field based heading estimation for pedestrian navigation environments. In: Indoor Positioning and Indoor Navigation (IPIN), 2011 International Conference on, IEEE, pp 1–10
- Alvarez H, Paz LM, Sturm J, Cremers D (2016) Collision Avoidance for Quadrotors with a Monocular Camera, Springer International Publishing, Cham, pp 195–209. DOI 10.1007/978-3-319-23778-7_14, URL http://dx.doi.org/10.1007/978-3-319-23778-7_14
- Amrita LP, Kumar AAN (2016) Bluetooth rssi based collision avoidance in multirobot environment. In: 2016 International Conference on Advances in Computing, Communications and Informatics (ICACCI), pp 2168–2174, DOI 10.1109/ICACCI.2016.7732373
- Basiri M (2015) Audio-based positioning and target localization for swarms of micro aerial vehicles
- Basiri M, Schill F, Floreano D, Lima PU (2014) Audio-based localization for swarms of micro air vehicles. In: Robotics and Automation (ICRA), 2014 IEEE International Conference on, IEEE, pp 4729–4734
- Basiri M, Schill F, Lima P, Floreano D (2016) On-board relative bearing estimation for teams of drones using sound. IEEE Robotics and Automation Letters 1(2):820–827
- Beard RW (2007) State estimation for micro air vehicles. In: Innovations in Intelligent Machines-1, Springer, pp 173–199
- Brambilla M, Ferrante E, Birattari M, Dorigo M (2013) Swarm robotics: a review from the swarm engineering perspective. Swarm Intelligence 7(1):1–41, DOI 10.1007/s11721-012-0075-2, URL <http://dx.doi.org/10.1007/s11721-012-0075-2>
- Caron C, Chamberland-Tremblay D, Lapierre C, Hadaya P, Roche S, Saada M (2008) Indoor positioning. In: Encyclopedia of GIS, Springer, pp 553–559
- Choudhry V, Singh R, Gehlot A (2017) RSSI-Based Indoor Robot Localization System Using LabVIEW, Springer Singapore, Singapore, pp 267–277. DOI 10.1007/978-981-10-1708-7_31, URL http://dx.doi.org/10.1007/978-981-10-1708-7_31
- Conroy P, Bareiss D, Beall M, van den Berg J (2014) 3-d reciprocal collision avoidance on physical quadrotor helicopters with on-board sensing for relative positioning. arXiv preprint arXiv:14113794
- Cornejo A, Nagpal R (2015) Distributed range-based relative localization of robot swarms. In: Algorithmic Foundations of Robotics XI, Springer, pp 91–107
- De Silva O, Mann GK, Gosine RG, et al (2014) Relative localization with symmetry preserving observers. In: Electrical and Computer Engineering (CCECE), 2014 IEEE 27th Canadian Conference on, IEEE, pp 1–6
- Dekking FM (2005) A Modern Introduction to Probability and Statistics: Understanding why and how. Springer Science & Business Media
- Faigl J, Krajcnik T, Chudoba J, Preucil L, Saska M (2013) Low-cost embedded system for relative localization in robotic swarms. In: Robotics and Automation (ICRA), 2013 IEEE International Conference on, IEEE, pp 993–998
- Fiorini P, Shiller Z (1998) Motion planning in dynamic environments using velocity obstacles. The International Journal of Robotics Research 17(7):760–772
- Gaugel T, Mittag J, Hartenstein H, Papanastasiou S, Strom EG (2013) In-depth analysis and evaluation of self-organizing tdma. In: Vehicular Networking Conference (VNC), 2013 IEEE, IEEE, pp 79–86
- Guo K, Qiu Z, Meng W, Nguyen TM, Xie L (2016a) Relative localization for quadcopters using ultra-wideband sensors. In: IMAV 2016: International Micro Air Vehicle Conference and Competition 2016, Beijing, China, October 17–21, 2016
- Guo K, Qiu Z, Miao C, Zaini AH, Chen CL, Meng W, Xie L (2016b) Ultra-wideband-based localization for quadcopter navigation. Unmanned Systems 04(01):23–34, DOI 10.1142/S2301385016400033, URL <http://www.worldscientific.com/doi/abs/10.1142/S2301385016400033>, <http://www.worldscientific.com/doi/pdf/10.1142/S2301385016400033>
- Ho H, De Wagter C, Remes B, de Croon G (2015) Optical-flow based self-supervised learning of obstacle appearance applied to mav landing. arXiv preprint arXiv:150901423
- Kallapur A, Petersen I, Anavatti S (2009) A discrete-time robust extended kalman filter. In: American Control Conference, 2009. ACC'09., IEEE, pp 3819–3823
- Kendoul F, Fantoni I, Nonami K (2009a) Optic flow-based vision system for autonomous 3d localization and control of small aerial vehicles. Robotics and Autonomous Systems 57(6):591–602
- Kendoul F, Nonami K, Fantoni I, Lozano R (2009b) An adaptive vision-based autopilot for mini flying machines guidance, navigation and control. Autonomous Robots 27(3):165–188
- Koenig N, Howard A (2004) Design and use paradigms for gazebo, an open-source multi-robot simulator. In: Intelligent Robots and Systems, 2004.(IROS 2004). Proceedings. 2004 IEEE/RSJ International Conference on, IEEE, vol 3, pp 2149–2154
- Kumar V, Michael N (2012) Opportunities and challenges with autonomous micro aerial vehicles. The International Journal of Robotics Research 31(11):1279–1291
- Kushki A, Plataniotis K, Venetsanopoulos A (2008) Indoor positioning with wireless local area networks (wlan). In: Encyclopedia of GIS, Springer, pp 566–571
- Labs S (2016) Bled112 bluetooth smart dongle. URL <https://www.bluegiga.com/en-US/products/bled112-bluetooth-smart-dongle>
- Ledergerber A, Hamer M, D'Andrea R (2015) A robot self-localization system using one-way ultra-wideband communication. In: Intelligent Robots and Systems (IROS), 2015 IEEE/RSJ International Conference on, IEEE, pp 3131–3137
- Lehnert C, Corke P (2013) μ av-design and implementation of an open source micro quadrotor. AC on Robotics and Automation, Eds
- Malyavej V, Kumkeaw W, Aorpimai M (2013) Indoor robot localization by rssi/imu sensor fusion. In: Electrical Engineering/Electronics, Computer, Telecommunications and Information Technology (ECTI-CON), 2013 10th International Conference on, IEEE, pp 1–6
- Martinelli A, Siegwart R (2005) Observability analysis for mobile robot localization. In: Intelligent Robots and Systems, 2005.(IROS 2005). 2005 IEEE/RSJ International Conference on, IEEE, pp 1471–1476
- Martinelli A, Pont F, Siegwart R (2005) Multi-robot localization using relative observations. In: Robotics and Automation, 2005. ICRA 2005. Proceedings of the 2005 IEEE International Conference on, IEEE, pp 2797–2802
- McGuire K, de Croon G, de Wagter C, Remes B, Tuyls K, Kappen H (2016) Local histogram matching for efficient optical flow computation applied to velocity estimation on pocket drones. In: 2016 IEEE International Conference on Robotics and Automation (ICRA), pp 3255–3260, DOI 10.1109/ICRA.2016.7487496
- Meyer J, Sendobry A, Kohlbrecher S, Klingauf U, Von Stryk O (2012) Comprehensive simulation of quadrotor uavs using ros and gazebo. In: Simulation, Modeling, and Programming for Autonomous Robots, Springer, pp 400–411
- Michael N, Mellinger D, Lindsey Q, Kumar V (2010) The grasp multiple micro-uav testbed. Robotics & Automation Magazine, IEEE 17(3):56–65
- Min S, Nam H (2016) A formation flight control of uavs using zigbee. In: 2016 13th International Conference on Ubiquitous Robots and Ambient Intelligence (URAI), pp 163–165, DOI 10.1109/URAI.2016.7625728

- Mueller M, Drouin A (2007) Paparazzithe free autopilot. build your own uav. In: 24th Chaos Communication Congress, Berliner Congress Center, Dec, pp 27–30
- Mulgaonkar Y, Cross G, Kumar V (2015) Design of small, safe and robust quadrotor swarms. In: Robotics and Automation (ICRA), 2015 IEEE International Conference on, IEEE, pp 2208–2215
- Nageli T, Conte C, Domahidi A, Morari M, Hilliges O (2014) Environment-independent formation flight for micro aerial vehicles. In: Intelligent Robots and Systems (IROS 2014), 2014 IEEE/RSJ International Conference on, IEEE, pp 1141–1146
- Nguyen K, Luo Z (2013) Evaluation of bluetooth properties for indoor localisation. In: Progress in Location-Based Services, Springer, pp 127–149
- No H, Cho A, Kee C (2015) Attitude estimation method for small uav under accelerative environment. *GPS Solutions* 19(3):343–355
- Parrot (2012) Ar drone 2.0. URL <http://ardrone2.parrot.com>
- Powers C, Mellinger D, Kushleyev A, Kothmann B, Kumar V (2013) Influence of aerodynamics and proximity effects in quadrotor flight. In: Experimental Robotics, Springer, pp 289–302
- Pulse (2008) W1049b datasheet version 1.1. URL www.cdiweb.com/datasheets/pulse/W1049B.pdf, accessed November 2015
- Quigley M, Conley K, Gerkey B, Faust J, Foote T, Leibs J, Wheeler R, Ng AY (2009) Ros: an open-source robot operating system. In: ICRA workshop on open source software, vol 3, p 5
- Remes B, Esden-Tempski P, Van Tienen F, Smeur E, De Wagter C, De Croon G (2014) Lisa-s 2.8 g autopilot for gps-based flight of mavs. In: IMAV 2014: International Micro Air Vehicle Conference and Competition 2014, Delft, The Netherlands, August 12-15, 2014, Delft University of Technology
- Roberts JF, Stirling T, Zufferey JC, Floreano D (2012) 3-d relative positioning sensor for indoor flying robots. *Autonomous Robots* 33(1-2):5–20
- Roelofsen S, Gillet D, Martinoli A (2015) Reciprocal collision avoidance for quadrotors using on-board visual detection. In: Intelligent Robots and Systems (IROS), 2015 IEEE/RSJ International Conference on, IEEE, pp 4810–4817
- Sabatini AM, Genovese V (2013) A stochastic approach to noise modeling for barometric altimeters. *Sensors* 13(11):15,692–15,707
- Sasiadek J, Wang Q (1999) Sensor fusion based on fuzzy kalman filtering for autonomous robot vehicle. In: Robotics and Automation, 1999. Proceedings. 1999 IEEE International Conference on, IEEE, vol 4, pp 2970–2975
- Scaramuzza D, Achtelik MC, Doitsidis L, Friedrich F, Kosmatopoulos E, Martinelli A, Achtelik MW, Chli M, Chatzichristofis S, Kneip L, et al (2014) Vision-controlled micro flying robots: from system design to autonomous navigation and mapping in gps-denied environments. *Robotics & Automation Magazine, IEEE* 21(3):26–40
- Seybold JS (2005) Introduction to RF propagation. John Wiley & Sons
- Shilov K (2014) The next generation design of autonomous mav flight control system smartap. In: IMAV 2014: International Micro Air Vehicle Conference and Competition 2014, Delft, The Netherlands, August 12-15, 2014, Delft University of Technology
- Snape J, van den Berg J, Guy SJ, Manocha D (2009) Independent navigation of multiple mobile robots with hybrid reciprocal velocity obstacles. In: Intelligent Robots and Systems, 2009. IROS 2009. IEEE/RSJ International Conference on, IEEE, pp 5917–5922
- Snape J, van den Berg J, Guy SJ, Manocha D (2011) The hybrid reciprocal velocity obstacle. *Robotics, IEEE Transactions on* 27(4):696–706
- Svečko J, Malajner M, Gleich D (2015) Distance estimation using rssi and particle filter. *ISA transactions* 55:275–285
- Szabo T (2015) Autonomous collision avoidance for swarms of mavs based solely on rssi measurements. Master's thesis, Delft University of Technology
- Townsend K, Cuff C, Davidson R, et al (2014) Getting started with Bluetooth low energy: Tools and techniques for low-power network- ing. O'Reilly Media, Inc.
- Van Den Berg J, Guy SJ, Lin M, Manocha D (2011) Reciprocal n-body collision avoidance. In: Robotics research, Springer, pp 3–19
- Vásárhelyi G, Virágh C, Somorjai G, Tarcai N, Szörényi T, Nepusz T, Vicsek T (2014) Outdoor flocking and formation flight with autonomous aerial robots. In: 2014 IEEE/RSJ International Conference on Intelligent Robots and Systems, IEEE, pp 3866–3873
- Wilkie D, Van den Berg J, Manocha D (2009) Generalized velocity obstacles. In: Intelligent Robots and Systems, 2009. IROS 2009. IEEE/RSJ International Conference on, IEEE, pp 5573–5578